Int. J. Multiphase Flow, Vol. 1, pp. 491–511. Pergamon Press, 1974. Printed in Great Britain.

THE TERMINAL SPEED OF SINGLE DROPS OR BUBBLES IN AN INFINITE MEDIUM

GRAHAM B. WALLIS

Thayer School of Engineering, Dartmouth College, Hanover, N.H. 03755 (U.S.A.)

(Received October 24, 1973)

Summary

This paper synthesises previous studies of the terminal speed of single drops or bubbles to provide a universal calculational procedure.

Introduction

The purpose of this paper is to present a straightforward correlating scheme for calculating the terminal velocity of single drops or bubbles acted on by a gravitational field in an infinite medium. The terminal velocity of a single particle is of interest in many practical applications (*e.g.*, atmospheric fallout, oil drops released by seepage under water, aeration of lakes) and also provides a starting point for the analysis of the flow of suspensions in pipes, fluidised beds, hindered settling, bubble columns and numerous other systems.

A great deal of work has been done in this field. However, previous authors have been concerned with a limited range of parameters and have presented their results with an often bewildering array of various dimensionless groups. Correlations derived by different authors are sometimes incompatible or are hard to compare because of the method of presentation. Thus there is a need for a survey which presents the significant past work on a common basis and with an economy of complexity (some previous surveys, such as Harper's [1], have been addressed largely to applied mathematicians). The emphasis of this work is on utility, convenience and brevity, while attempting to offer sufficient explanation and evidence to convince the reader that the results are reasonable.

It is intended that these results will provide an improvement over the work of Peebles and Garber [2], which is recommended in ref. [3] for calculating bubble rise velocities, and achieve consolidation by treating bubbles and drops simultaneously. In addition, by presenting results for a large variety of systems on a common scale a perspective will be obtained of the confidence with which practical performance can be predicted.

A solid spherical particle

The usual method for deriving the terminal speed of a spherical particle falling (or rising) under gravity is to consider the balance between buoyancy and drag forces. Employing the drag coefficient for a particle in an infinite medium, $C_{D\infty}$, we have

$$\frac{4}{3}\pi r^3 g\Delta\rho = C_{D\infty}\,\pi r^2 \frac{1}{2}\rho_f v_\infty^2 \tag{1}$$

$\Delta\rho$ is the density difference, v_∞ the terminal speed, ρ_f the density of the surrounding fluid and r the particle radius. The drag coefficient is a function of the Reynolds Number,

$$Re_\infty = \frac{2\rho_f v_\infty r}{\mu_f} \tag{2}$$

Since both v_∞ and r appear in each of eqns. (1) and (2), the dependence of terminal speed on size must usually be determined by iteration. A more direct approach is to combine eqns. (1) and (2) to generate dimensionless forms of the speed and radius which only contain one of these variables, thus

$$v^* = \left(\frac{4}{3}\frac{Re_\infty}{C_{D\infty}}\right)^{1/3} = v_\infty \left(\frac{\rho_f^2}{\mu_f g\Delta\rho}\right)^{1/3} \tag{3}$$

$$r^* = \left(\frac{3}{32} C_{D\infty} Re_\infty^2\right)^{1/3} = r\left(\frac{\rho_f g\Delta\rho}{\mu_f^2}\right)^{1/3} \tag{4}$$

If the relationship between $C_{D\infty}$ and Re_∞ is known, v^* may be directly related to r^*, as shown in Fig. 1.

For computational purposes it may be more convenient to have an analytical correlation. We therefore approximate the curve in Fig. 1 by four segments, each representing a straight line on log paper, as shown in Table 1.

These lines have not been chosen "optimally" to minimise deviation from the drag coefficient curve but for convenience in estimating velocities to within 10% accuracy, it being realised that fluid properties and particle dimensions are usually not known well enough to justify greater precision.

TABLE 1

General correlation for terminal speed of spherical particles

Region	Equation	Range
1	$v^* = \frac{2}{9} r^{*2}$	$r^* < 1.5,\ v^* < 0.5$
2	$v^* = 0.307\, r^{*1.21}$	$1.5 < r^* < 10,\ 0.5 < v^* < 5$
2B	$v^* = 0.693\, r^{*0.858}$	$10 < r^* < 36,\ 5 < v^* < 15$
2C	$v^* = 2.5\, r^{*1/2}$	$36 < r^*,\ 15 < v^*$

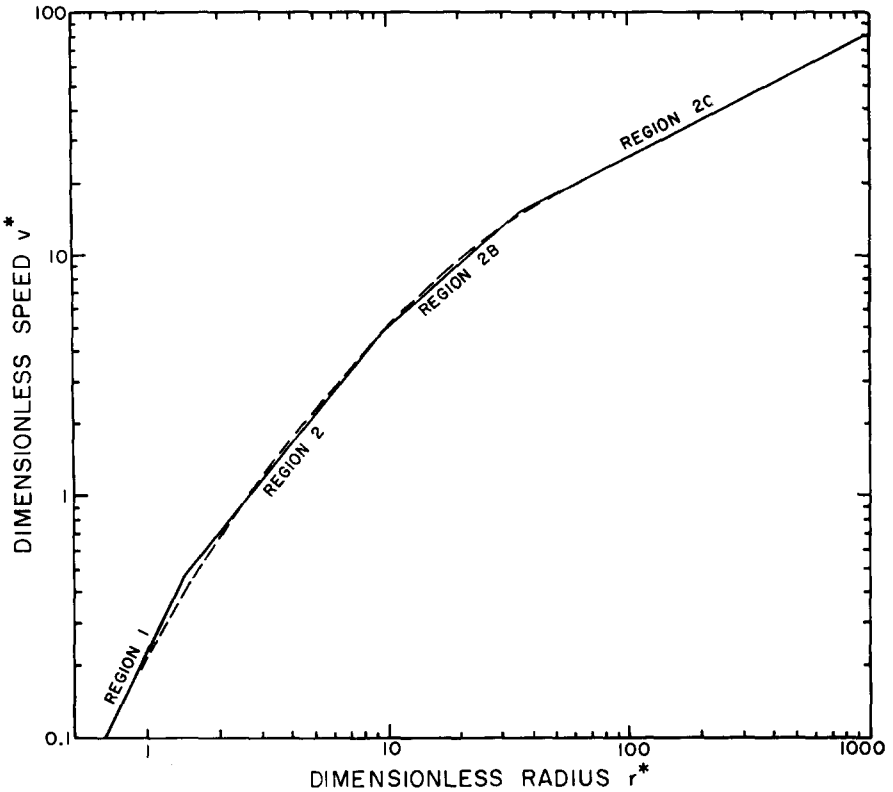

Fig. 1. Dimensionless representation of terminal speed of solid spheres. Dashed curve derived from ref. [9].

The four subdivisions actually have physical significance. Region 1 is a regime of entirely viscous flow; in Region 2 inertia forces become important; Region 2B reflects the effect of vortex shedding, while Region 2C corresponds to a fully-developed turbulent wake. Values of r^* greater than 1000, which are needed to bring about the sudden drop in drag coefficient which occurs above $Re_\infty = 2 \times 10^5$, are far higher than are usually encountered in practice.

Should an interpretation of the various regimes be desired in terms of the conventional Reynolds Number we can combine eqns. (3) and (4) to get

$$Re_\infty = 2 v^* r^*$$

The breakpoints between the various regions in Table 1 are then at Re_∞ = 1.5, 100 and 1080, respectively.

A correlation scheme in this form, though particularly convenient, does not seem to be in common use at present. However, there is a precedent for a similar method in the work of Hughes and Gilliland [4], while Graf [5] discusses the possibility of such an approach, based on the paper by Schiller and Naumann [6], without deriving explicit results. Baker and Chao [7] and also Licht and Narasimhamurty [8] mention a similar technique.

Drops and bubbles

The case of drops and bubbles is complicated by the additional action of two major variables and several minor ones.

The major new phenomena are:

(a) surface tension, which influences the particle shape;

(b) cleanliness, which influences the boundary condition at the interface and may exert a critical effect on stability.

The minor variables include the viscosity and density of the fluid inside the drop or bubble.

In order to account for surface tension we must introduce one more dimensionless group. For example, this could be the Weber Number

$$\mathrm{We} = \frac{2\rho_c v_\infty^2 r}{\sigma} \tag{6}$$

which represents a balance between surface tension and inertia effects. The Weber Number is in common use for describing the stability of drops in gas streams.

Since we wish to develop common equations for drops and bubbles, as much as possible, we shall use the subscripts c and d to denote the continuous and discontinuous phases, respectively. $\Delta\rho$ will represent the magnitude of the density difference. Equations (3) and (4) then become

$$v^* = v_\infty \left(\frac{\rho_c^2}{\mu_c g \Delta\rho}\right)^{1/3} \tag{7}$$

$$r^* = r \left(\frac{\rho_c g \Delta\rho}{\mu_c^2}\right)^{1/3} \tag{8}$$

The various dimensionless groups can be combined to produce new combinations which are particularly convenient. For instance, we may eliminate both v_∞ and r by combining r^*, v^* and We to get a group called the "Archimedes Number" in ref. [3],

$$N_{\mathrm{Ar}} = \left(\frac{\sigma^3 \rho_c^2}{\mu_c^4 g \Delta\rho}\right)^{1/2} \tag{9}$$

This number is a constant for a given two-fluid system. It has the same significance as the "property group" ($Y = g\mu_f^4/\rho_f\sigma^3$) used by White and Beardmore [10], the parameter *Sd* used by Hughes and Gilliland [4], the "M Number" used by Haberman and Morton [11] and by Moore [12, 13], the group G_1 used by Peebles and Garber [2], and the parameter P used by Hu and Kintner [14].

Since $\mathrm{P} = N_{\mathrm{Ar}}^2$ and is perhaps more well known than N_{Ar} it will be used in the rest of this paper. Explicitly, we have

$$\mathrm{P} = \frac{\sigma^3 \rho_c^2}{\mu_c^4 g \Delta\rho} \tag{10}$$

A dimensionless group which represents the balance between gravitational and surface tension forces is

$$B = \frac{g r^2 \Delta\rho}{\sigma} \tag{11}$$

which is variously known as the Bond Number, the Eötvös Number and the Laplace Number. Sometimes it is defined using the diameter instead of the radius, or as the square root of the expression given in eqn. (11).

A dimensionless velocity which is independent of viscosity or radius may be obtained by combining eqns. (7) and (10) to get

$$K = v^* P^{-1/12} = v_\infty \rho_c^{1/2} (g \sigma \Delta\rho)^{-1/4} \tag{12}$$

which has been called the Kutateladze Number, particularly when it describes a liquid phase surrounded by its own vapor.

If surface tension were the only variable distinguishing drops and bubbles from solid particles we should expect that a correlation of v^* *versus* r^* for various values of N_{Ar} or P would describe these systems. This is partly true, however; over a certain range of the parameters, "cleanliness" exerts a significant influence and appears to be the explanation for the scatter noted by numerous experimenters.

A general correlation scheme

Individual "regions" will first be presented, followed by a summary of overall results and conclusions.

Region 1 "Creeping flow"

If the drops or bubbles are sufficiently small ($r^* < 1.5$), viscous forces dominate inertia forces and the rise velocity can be predicted from the theory of "creeping flow" as long as the interface remains spherical [15, 16]. The classical result in this case is

$$v^* = \frac{2}{9} r^{*2} \left(\frac{3\mu_d + 3\mu_c}{3\mu_d + 2\mu_c} \right) \tag{13}$$

where μ_c is the viscosity of the continuous phase and μ_d the viscosity of the discontinuous phase. Equation (13) implies that bubbles ($\mu_c >> \mu_d$) would rise 50% faster than solid spheres and that the viscosity ratio would correlate data taken with different liquid—liquid systems.

There is a shortage of data taken in Region 1, most authors having worked with relatively inviscid fluids and with other than microscopic particles. In the case of bubbles, Haberman and Morton [11] concluded, from an examination of both their own data and previous work, that interfacial effects were far more important than internal viscosity in determining how far the bubbles behaved as "fluid spheres" with internal circulation. Slight amounts of impurities concentrated on the interface were apparently adequate

to give it sufficient rigidity to suppress internal circulation altogether. Sufficiently small bubbles in any liquid behaved as solid spheres. Bond and Newton [17] also found that small bubbles or drops behaved as solid spheres while larger ones obeyed eqn. (13).

Figure 2 shows some of Haberman and Morton's data in Region 1. Bubbles in mineral oil approach the "fluid sphere" line while in corn oil solutions the bubble interface is apparently rigid, perhaps due to the preferential concentration of certain molecules there.

The very small number of data points obtained by Peebles and Garber [2] in this region are also very close to the solid sphere line.

Unfortunately, the extensive data of Hu and Kintner [14] for drops of

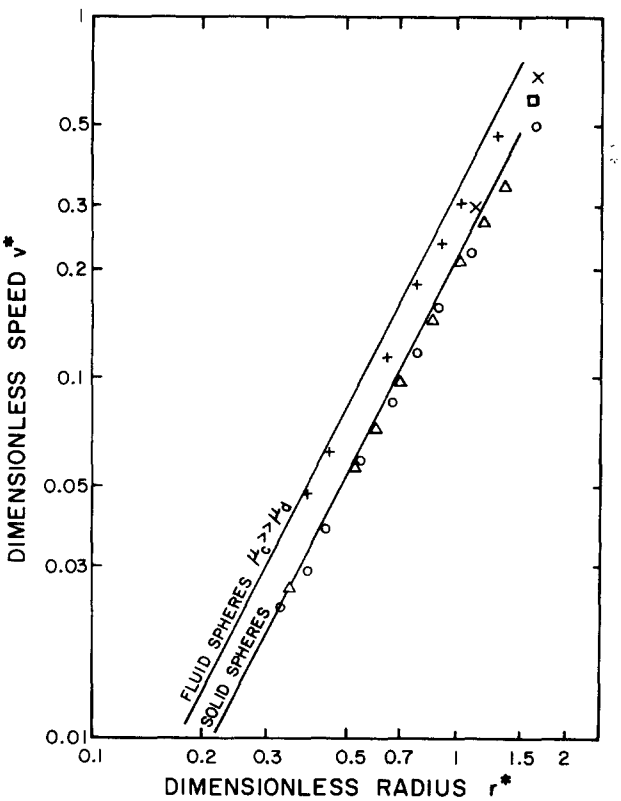

Fig. 2. Data for bubbles in Region 1.

various fluids in water were all obtained with $r^* > 1.5$, beyond the range included in Region 1.

It might be suspected that if surface tension forces were inadequate to maintain a spherical shape to the interface, eqn. (13) would cease to be valid. This might be the case for sufficiently small values of P but has not so far been observed in practice. Haberman and Morton [11] found that all bubbles in viscous fluids were spherical below about $r^* = 1$ in their experiments.

Region 2

Region 2 covers the range of dimensionless radii between $r^* = 1.5$ and $r^* = 10$. In this region, solid spheres are described approximately by the equation given in Table 1, namely,

$$v^* = 0.307\, r^{*1.21} \tag{14}$$

In their studies of air bubbles rising in various liquids, Haberman and Morton [11] found some agreement with eqn. (14). However, some velocities of rise were significantly above this prediction. Although the actual performance varied rather whimsically between the different fluids, an envelope could be drawn which gave an upper limit to the observed velocities. This upper bound can be represented by the "fluid sphere" line in Region 2, which we shall call Region 2A, with the equation

$$v^* = 0.408\, r^{*1.5} \tag{15}$$

Peebles and Garber [2] did not present upper and lower bounds in their paper but instead correlated their own data for bubbles rising in liquids, as well as data of Allen [18] and Datta, Napier and Newitt [19] with an equation which is equivalent to

$$v^* = 0.33\, r^{*1.28} \tag{16}$$

Equation (16) is intermediate between eqns. (14) and (15). Indeed, Peebles and Garber's data all lie between these limits, as shown in Fig. 3.

Hu and Kintner's data [14] for a large variety of liquid droplets in water are shown in Fig. 4. In Region 2 the data are generally slightly above the line representing eqn. (14) but well below the line corresponding to eqn. (15). Hu and Kintner's data are remarkably self-consistent in Fig. 4, although the ratio μ_c/μ_d varied from 0.1 to almost 2, and follow the "solid spheres" line closely in Region 2.

Figure 4 also shows that water drops falling in air [20] behave approximately as solid spheres in this region.

Regions 2B, 2C and 2D

As long as the surface tension is sufficiently large, bubbles and drops continue to behave as spheres when r^* is increased above 10. Thus, in Fig. 4, most of the dispersed drop systems studied by Hu and Kintner follow the equation describing region 2B in Table 1 until they become too large to

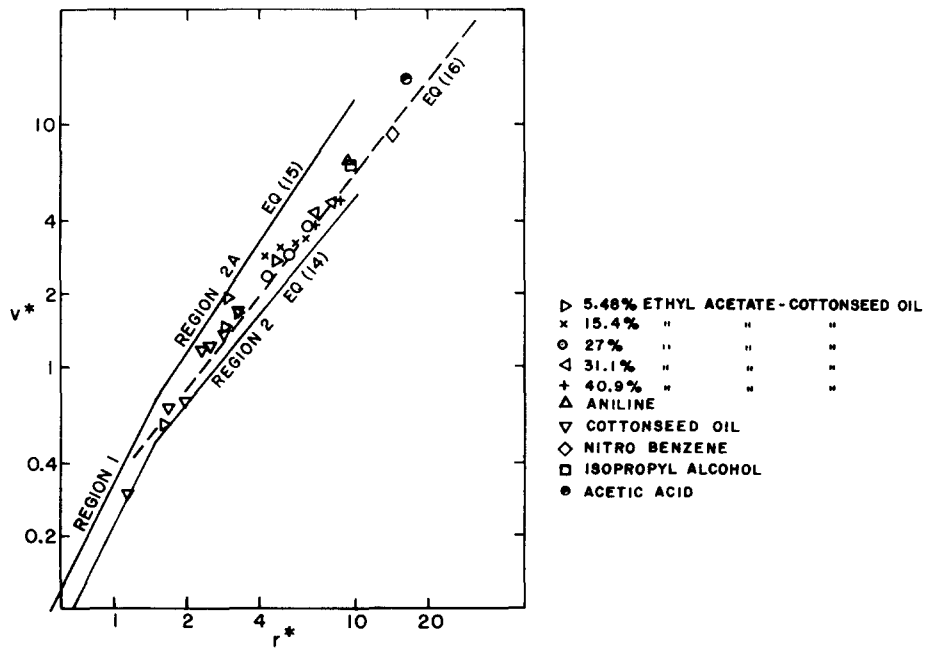

Fig. 3. Region 2. Data of Peebles and Garber [2] for bubbles rising in various liquids.

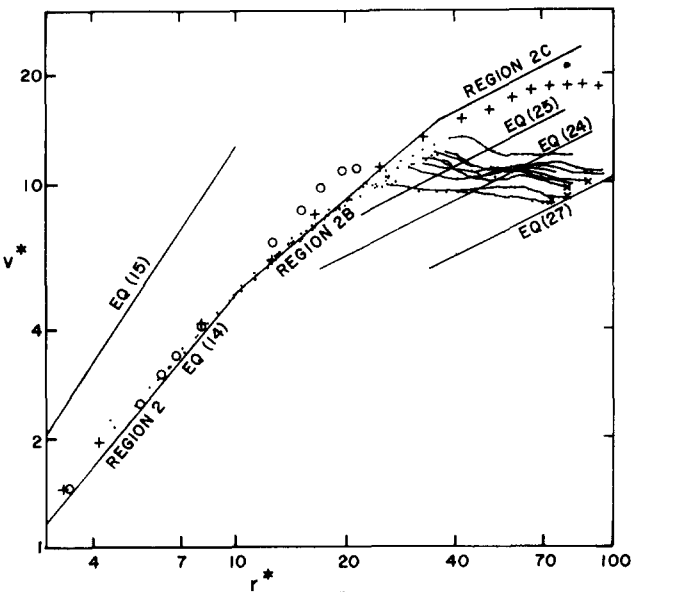

Fig. 4. Regions 2, 2B and 2C.

remain spherical and their drag coefficients increase. Water drops in air behave similarly. Only the aniline droplets used by Hu and Kintner depart significantly from the "solid spheres" curve.

The "fluid spheres" curve can also be continued beyond $r^* = 10$. The extensive work of Moore [12, 13] led to the predictions shown in Fig. 5.

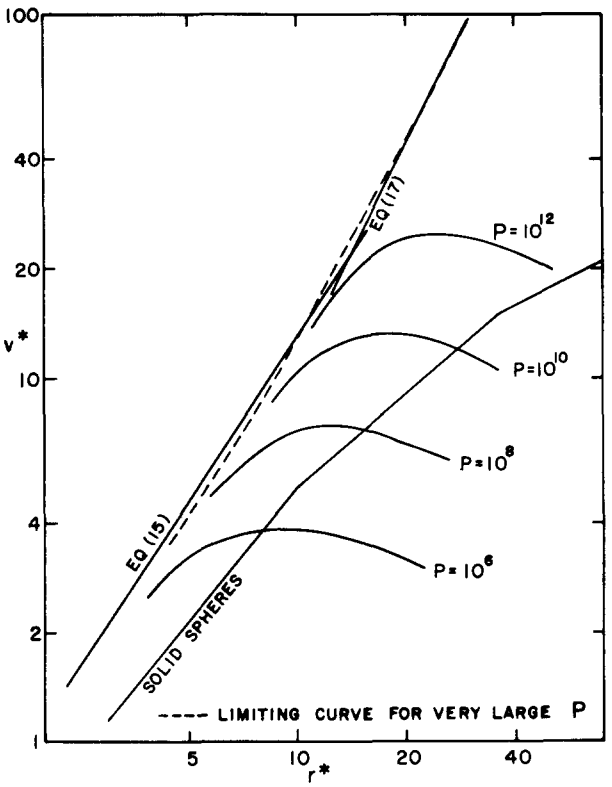

Fig. 5. Moore's predictions for fluid spheres [12, 13].

For very large values of P, Moore's results agree fairly well with eqn. (15) up to $r^* = 10$ and have a limit at large r^* corresponding to $C_{D\infty} = 48/\mathrm{Re}_\infty$, which is equivalent to

$$v^* = \frac{r^{*2}}{9} \tag{17}$$

A reasonable fit to Moore's entire curve for large P is obtained by using eqn. (15) up to $r^* = 13.4$, $v^* = 20$ and eqn. (17) thereafter.

For finite values of P, increase in radius eventually leads to interface distortion, oscillations, vortex-shedding, etc., all of which combine to enhance the drag. Some of Moore's predictions for finite P are shown in Fig. 5. The limit on the right-hand end of these curves is a constant value of Weber

Number, predicted by Moore to be 3.75, which corresponds to a new Region 3. Haberman and Morton's data for air bubbles rising in Varsol, methyl alcohol and turpentine are close to Moore's predictions in this region. Other data fall below Moore's curves but above the "solid sphere" lines.

Apparently, no combination of fluids yet tested has had a high enough P number for data to be taken to compare with eqn. (17). However, there appears to be evidence of an intermediate regime (2D), perhaps for systems which are not quite clean enough to behave entirely as "fluid spheres", which obeys an equation of similar form. Haberman and Morton's data for bubbles rising in distilled water, (Fig. 6), follow quite closely the line

$$v^* = \frac{2}{27} r^{*2} \tag{18}$$

corresponding to a drag coefficient of $C_{D\infty} = 72/\mathrm{Re}_\infty$. (In impure water the "solid sphere" line is followed.) Similarly, data of Thorsen *et al.* [21] for drops of *o*-dichlorobenzene, carbon tetrachloride or ethylene bromide falling in water follow the line

$$v^* = 0.05\, r^{*2} \tag{19}$$

in this region (Fig. 7). The drag coefficient in this case is $C_{D\infty} = 107/\mathrm{Re}_\infty$.

Other data taken by Thorsen *et al.* for a variety of liquid—liquid systems either agree with the "solid sphere" line or lie between it and eqn. (19). In some cases there is a distinct discontinuity in behavior (Fig. 7). The results appear to be very sensitive to the "cleanliness" of the system and its effect on interfacial phenomena.

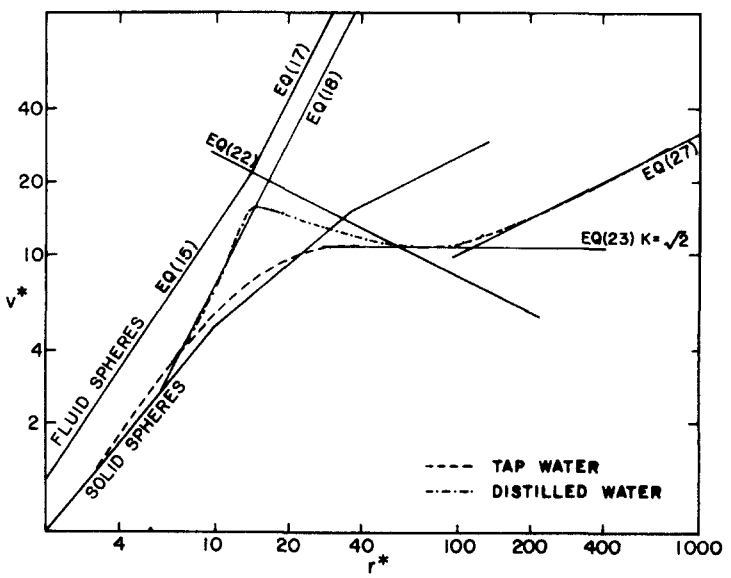

Fig. 6. Air bubbles rising in water (Haberman and Morton [11]).

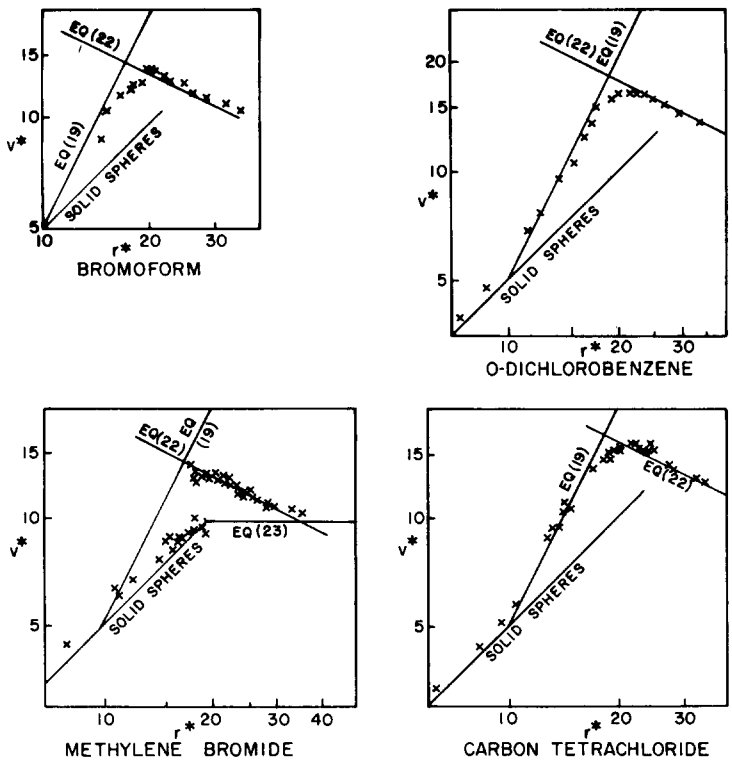

Fig. 7. Terminal velocities of liquid drops in water [21] showing Regions 2D and 3.

Similar conclusions can be reached from the work of Licht and Narasimhamurty [8], who studied the terminal velocities in water of droplets of six different liquids. In Region 2B most of their results were close to the "rigid sphere" line. However, ethyl chloroacetate drops gave results closer to eqn. (19).

Region 3

In Region 3 the shape of bubbles or drops departs significantly from sphericity, they move in helical or zig-zag paths, and the velocity decreases as the "effective radius", r, increases. The effective radius is the radius of a sphere which would have the same volume as the dispersed globule.

Several authors have identified this region as characterised by a constant value of Weber Number. Moore gives the value 3.745, Peebles and Garber 3.65 for bubbles [2], Hu and Kintner 3.58 for drops [14], Winnikow and Chao 4.08 for drops [22]. Thorsen *et al.* [21], working with liquid drops falling in water obtained

$$We = \left(\frac{6.8}{1.65 - \frac{\Delta\rho}{\rho_d}}\right)^2 \frac{1}{3\,\frac{\rho_d}{\rho_c} + 2} \qquad (20)$$

However, over the range actually studied by these authors a mean value of We = 4 represents the data within experimental accuracy (Fig. 7).

Since various factors can reduce the velocity below the value given by eqn. (20), a reasonable upper limit to take is We = 4, or, if a direct equation for v_∞ is desired,

$$v_\infty = \left(\frac{2\sigma}{\rho_c r} \right)^{1/2} \tag{21}$$

which is equivalent to

$$v^\star = \sqrt{2}\, r^{\star -1/2}\, P^{1/6} \tag{22}$$

The only data which appear to give higher values than these predictions in Region 3 are the recent results of Edge and Grant [23]. However, the apparent inconsistency is due to their unusual definition of We.

The results of Licht and Narasimhamurty [8], who studied liquid drops falling in water for values of P between 3.35×10^9 and 6.8×10^{10}, are almost all within 10% of eqn. (22) in Region 3 with the tendency being for the data points to follow smooth curves rather than sudden transitions between regimes. Thus the first onset of zig-zag motion and departure from Region 2 occurs at a Weber Number rather less than 4 (approximately 2 or 3) [24, 25, 26] with a short transition from there to Region 3 as $r^\star$ is increased.

Region 4

In Region 4 the bubble or drop velocity is independent of size and corresponds to a constant value of K (defined by eqn. (12)). For bubbles, Peebles and Garber [2] give K = 1.18, a value which is probably too low due to the influence of the proximity of the walls of their vessel on the larger bubbles. Harmathy [27] gives K = 1.53 for bubbles. Levich [28] and Mendelson [29] give $K = \sqrt{2}$. Kutateladze [30] gives K = 1.28 for drops. Haberman and Morton's data for air bubbles in water [11] support the value $\sqrt{2}$. Hu and Kintner's extensive data [14] for drops (see the right-hand side of Fig. 4) give K between 1.39 and 1.57 with an average of 1.48. Water drops falling in air (the data shown in Fig. 4) have a maximum velocity corresponding to K = 1.97 but the data do not extend to large enough values of $r^\star$ to be clearly in Region 4. The drops may also not have fallen far enough to develop a "fully-distorted" shape.

The chosen value depends to some extent on the method of definition. $K = \sqrt{2}$ probably represents the minimum velocity between Regions 3 and 5, whereas a slightly higher value does a better job of correlating data which include the transition between regions.

In terms of the dimensionless velocity and radius defined earlier we may write, for Region 4,

$$v^\star = K P^{1/12} \tag{23}$$

with a recommended value of $K = \sqrt{2}$ for the "true" minimum or inflection point in curves such as those shown in Fig. 6, while $K = 1.56$ correlates data within about 10% over a wider range of r^*.

It is easily checked that Regions 3 and 4 meet on the line

$$v^{*2} = 2r^* \qquad \text{for } K = \sqrt{2} \tag{24}$$

or

$$v^{*2} = 3r^* \qquad \text{for } K = 1.56 \text{ or } 6^{0.25} \tag{25}$$

The transitions between Regions 3 and 4 in Fig. 4 can be seen to lie between the lines representing eqns. (24) and (25).

The Bond Number at the intersection between Regions 3 and 4 has the value $4/K^4$, *i.e.* 1 if $K = \sqrt{2}$ and 2/3 if $K = 6^{0.25}$.

It is not clear whether cleanliness or the minor variables of viscosity or density ratio have any significant influence in this region.

Region 5

Very large bubbles assume a "spherical cap" shape with a flat base. Both viscous and surface tension forces can be neglected and the rise velocity is given by a balance between form drag and buoyancy. The analytical result derived by Davies and Taylor [31] for this regime is equivalent to

$$v_\infty = \sqrt{\frac{g r \Delta\rho}{\rho_c}} \tag{26}$$

or

$$v^* = r^{*1/2} \tag{27}$$

(Some authors give $v^* = 1.02\, r^{*1/2}$ but the 2% difference is unimportant in practice and the simpler expression is preferable.)

Equation (27) has been confirmed for several systems. Figure 6 shows close agreement for air bubbles in water. Davenport *et al.* [32] studied spherical cap bubbles of air rising through mercury in tubes 15 cm in diameter. Their results agree with eqn. (27) if the correction for finite tube radius, R, given by Wallis [33] is used, *i.e.*

$$\frac{r}{R} < \frac{1}{8} \qquad \frac{v_b}{v_\infty} = 1 \tag{28}$$

$$\frac{1}{8} < \frac{r}{R} < 0.6 \qquad \frac{v_b}{v_\infty} = 1.13\, e^{-r/R} \tag{29}$$

Comparison between theory and experiment is shown in Fig. 8.

The transition between Regions 4 and 5 occurs at We = 8, B = 4 for $K = \sqrt{2}$ in Region 4 (or We = 12, B = 6 if K = 1.56). Thus the values of bubble radii at the beginning and end of Region 4 only differ by a factor of 2 or 3.

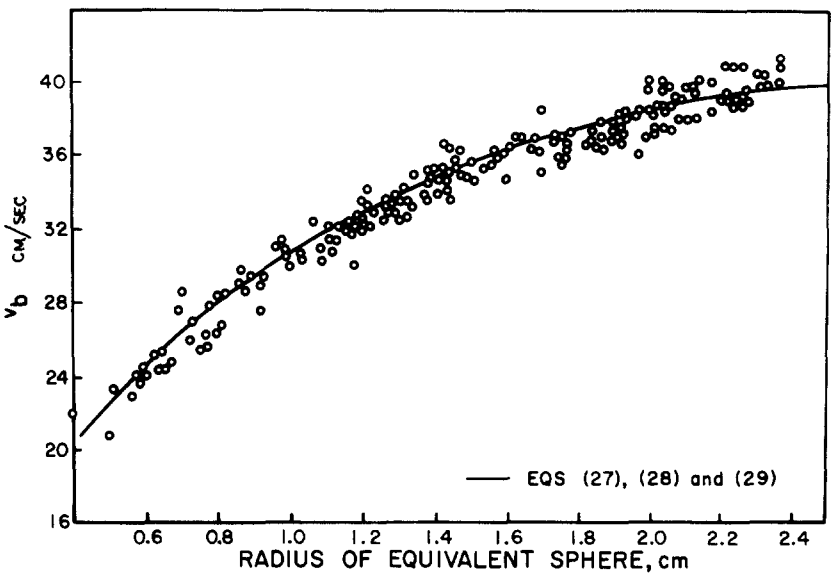

Fig. 8. Air bubbles rising through mercury in Region 5 (ref. [32]).

However, Region 4 has significant practical importance since bubbles which are released from porous plates or wettable horizontal surfaces tend to have Bond Numbers within this range.

Unlike bubbles, drops appear to have no Region 5, becoming unstable and breaking up at about the Weber Number (or Bond Number) characteristic of the upper limit of Region 4. Hu and Kintner [14] increased the volume of their droplets until they reached this limit, which in most cases lay close to the predictions of eqn. (27) (Fig. 4).

Transition between the various regions

Very small droplets or bubbles obey eqn. (13), usually behaving approximately as solid spheres if they are small enough. Very large bubbles obey eqn. (27), which is also close to the condition for large drops to shatter. Thus the dimensionless variables r^* and v^* determine the behavior at both extremes. In between, the characteristics of a particular fluid combination depend both on the value of P and on the somewhat erratic parameter of "cleanliness".

At high values of P the normal sequence, as r^* is increased, is in ascending order of Regions, starting at 1 and ending at 5 as shown, for example, in Fig. 6. The presence of impurities may suppress Region 3, which usually provides an upper limit to rise velocity in its range of influence, leading to a direct transition from Region 2 to Region 4.

At lower values of P, Regions 3 and 4 become compressed between Regions 2 and 5, eventually disappearing completely below $P \approx 100$. For example, Fig. 9 shows a direct transition from Region 1 through Region 2A to Region 5 for air bubbles rising in mineral oil, and a similar transition for air bubbles rising in a 68% corn syrup solution. The same Figure shows a progression from Region 2 through Region 4 to Region 5 for bubbles rising in a 56% glycerin solution. For globules which behave as solid spheres the intersection between eqns. (24) and (14) shows that Region 3 will disappear for $P < 10^5$.

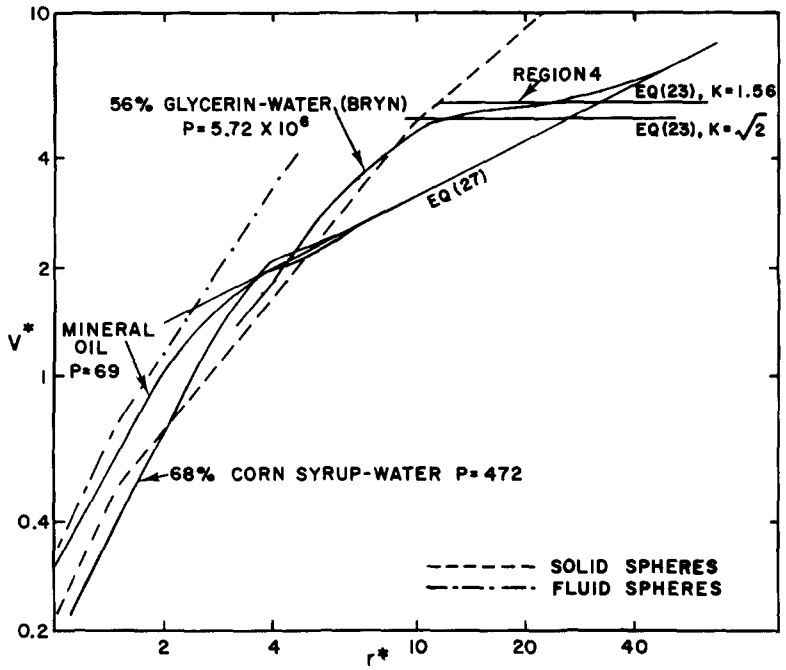

Fig. 9. Progressive disappearance of Regions 3 and 4 as the value of P is decreased (Haberman and Morton [11]).

Figure 10 presents all of the Regions on one graph, summarising these results, showing where the various regions of behavior can occur and the transitions between them.

Summary

Figure 10 summarises the results graphically by a plot of v^* *versus* r^* for various values of P. Algebraic expressions are available for all of the lines on the graph, as shown in Table 2.

Region 3 corresponds to a constant value of the Weber Number (We = 4) and meets Region 4 at a fixed value of Bond Number (B = 1).

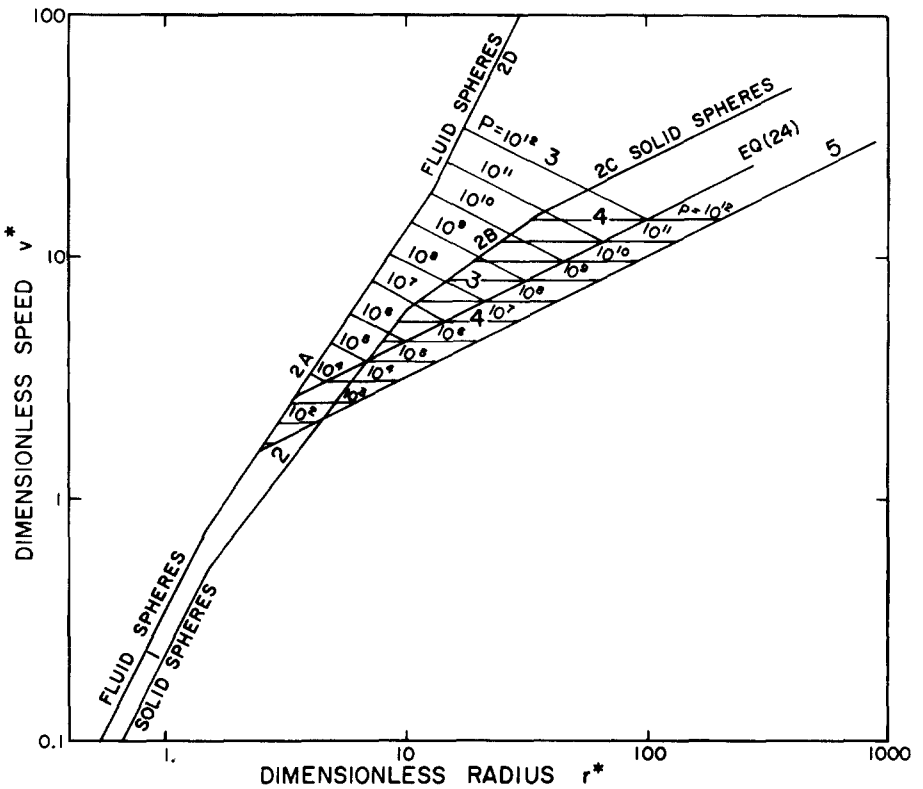

Fig. 10. Summary graph presenting all results. Behavior in Regions 3 and 4, which overlap, is strongly influenced by cleanliness.

Region 4 meets Region 5 at B = 4, We = 8.

In most practical cases the transitions between regions are not as sharp as the correlations indicate.

In all regions except Regions 4 and 5, fluid cleanliness exerts a strong influence, giving rise to significant uncertainties when making practical predictions. The expressions given in this paper, however, should serve to provide upper and lower bounds to the possible values of terminal speed.

Acknowledgments

The author received support from NSF Grant Number GK-35624 during the preparation of this paper. Some preliminary work on this topic was done by William E. Zimmer during a course at Dartmouth College.

TABLE 2

Region	Equation	Range
Solid spheres		
1	$v^* = \frac{2}{9} r^{*2}$	$r^* < 1.5, \quad v^* < 0.5$
2	$v^* = 0.307\, r^{*1.21}$	$1.5 < r^* < 10, \quad 0.5 < v^* < 5$
2B	$v^* = 0.693\, r^{*0.858}$	$10 < r^* < 36, \quad 5 < v^* < 15$
2C	$v^* = 2.5\, r^{*1/2}$	$36 < r^*, \quad 15 < v^*$
Fluid spheres ($\mu_c >> \mu_d$)		
1	$v^* = \frac{r^{*2}}{3}$	$r^* < 1.5, \quad v^* < 0.75$
2A	$v^* = 0.408\, r^{*1.5}$	$1.5 < r^* < 13.4, \quad 0.75 < v^* < 20$
2D	$\begin{cases} v^* = \frac{r^{*2}}{9} \\ \left(v^* = C r^{*2} \text{ where } C < \frac{1}{9}\right) \end{cases}$	$13.4 < r^*, \quad 20 < v^*$
3	$v^* = \sqrt{2}\, r^{*-1/2}\, P^{1/6}$	Between the "fluid sphere" lines and $v^{*2} = 2 r^*$
4	$v^* = \sqrt{2}\, P^{1/12}$	Between the "solid sphere" lines and Region 5
5	$v^* = r^{*1/2}$	Only valid for bubbles. Drops break up in this region

Nomenclature

C_{D^∞}	drag coefficient in an infinite medium
g	acceleration due to gravity
r	particle radius; radius of a sphere having the same volume as a drop or bubble
R	tube radius
v	terminal speed
μ	viscosity
ρ	density
$\Delta\rho$	density difference
σ	surface tension

Subscripts

b	bubble
c	continuous phase
d	discontinuous phase
f	fluid
∞	in an infinite medium

Dimensionless groups

B	$\frac{g r^2 \Delta\rho}{\sigma}$	"Bond Number"
K	$v_\infty \rho_c^{1/2} (g\sigma \Delta\rho)^{-1/4}$	"Kutateladze Number"
N_{Ar}	$\left(\frac{\sigma^3 \rho_c^2}{\mu_c^4 g\Delta\rho} \right)^{1/2}$	"Archimedes Number"
P	$\frac{\sigma^3 \rho_c^2}{\mu_c^4 g\Delta\rho}$	"Property Group" (N_{Ar}^2)
Re_∞	$\frac{2 \rho_c v_\infty r}{\mu_c}$	"Reynolds Number"
r^*	$r \left(\frac{\rho_c g\Delta\rho}{\mu_c^2} \right)^{1/3}$	"Dimensionless Radius"
v^*	$v_\infty \left(\frac{\rho_c^2}{\mu_c g\Delta\rho} \right)^{1/3}$	"Dimensionless Speed"
We	$\frac{2 \rho_c v_\infty^2 r}{\sigma}$	"Weber Number"

References

1 J.F. Harper, Advances in Applied Mechanics, Vol. 12, Academic Press, New York, 1972, pp. 59—129.
2 F.N. Peebles and H.J. Garber, Chem. Eng. Progr., 49 (1953) 88—97.
3 G.B. Wallis, One-Dimensional Two-Phase Flow, McGraw-Hill, New York, 1969, p. 250.
4 R.R. Hughes and E.R. Gilliland, Chem. Eng. Progr., 48 (1952) 497—504.
5 W.H. Graf, Hydraulics of Sediment Transport, McGraw-Hill, New York, 1971, p. 43.
6 L. Schiller and A. Naumann, Z. Ver. Deut. Ing., 77 (1933) 318—320.
7 J.L.L. Baker and B.T. Chao, Report No. AT(11-1)—1069, Univ. of Illinois, 1963.
8 W. Licht and G.S.R. Narasimhamurty, AIChE J., 1 (1955) 366—373.
9 R.B. Bird, W.E. Stewart and E.N. Lightfoot, Transport Phenomena, Wiley, New York, 1960, p. 192.
10 E.T. White and R.H. Beardmore, Chem. Eng. Sci., 17 (1962) 351—361.
11 W.L. Haberman and R.K. Morton, David W. Taylor Model Basin Report 802, 1953.
12 D.W. Moore, J. Fluid Mech., 23 (1965) 749—766.
13 D.W. Moore, J. Fluid Mech., 16 (1963) 161—176.
14 S. Hu and R.C. Kintner, AIChE J., 1 (1955) 42—48.
15 G.G. Stokes, Mathematical and Physical Papers, Vol. 1, Cambridge Univ. Press, London, 1880.
16 J. Hadamard, Compt. Rend. Acad. Sci. Paris, 152 (1911) 1735—1738.
17 W.N. Bond and D.A. Newton, Phil. Mag., 5 (1928) 794—800.
18 H.S. Allen, Phil. Mag., 50 (1900) 323—338.
19 R.L. Datta, D.H. Napier and D.M. Newitt, Trans. Inst. Chem. Eng., 28(3) (1950) 14—26.
20 W.R. Lane and H.L. Green, Surveys in Mechanics, Cambridge Univ. Press, London, 1956, pp. 162—215.

21 G. Thorsen, R.M. Stordalen and S.G. Terjesen, Chem. Eng. Sci., 23 (1968) 413—426.
22 S. Winnikow and B.T. Chao, Physics Fluids, 9 (1966) 50.
23 R.M. Edge and C.D. Grant, Chem. Eng. Sci., 26 (1971) 1001—1012.
24 P.G. Saffman, J. Fluid Mech., 1 (1956) 249—275.
25 R.A. Hartunian and W.R. Sears, J. Fluid Mech., 3 (1957) 27—47.
26 J.B. Haggard, Jr., NASA TN D—5809, 1970.
27 T.Z. Harmathy, AIChE J., 6 (1960) 281—288.
28 V.G. Levich, Physicochemical Hydrodynamics, Prentice-Hall, Englewood Cliffs, N.J., 1962.
29 H.D. Mendelson, AIChE J., 13 (1967) 250—253.
30 S.S. Kutateladze, Fluid Mech., Sov. Res., 1(4) (1972) 29—50.
31 R.M. Davies and G.I. Taylor, Proc. Roy. Soc., 200, Ser. A. (1950) 375—390.
32 W.G. Davenport, A.V. Bradshaw and F.D. Richardson, J. Iron Steel Inst., 205 (1967) 1034—1042.
33 G.B. Wallis, One-Dimensional Two-Phase Flow, McGraw-Hill, New York, 1969, p. 251.

Appendix

Examples

In order to illustrate the methods developed in this paper, several examples will be worked out in detail and compared with data which were not used to derive the correlations. Data will generally be chosen to correspond to "transition regions", thus providing a more severe test of the theory.

Example 1. Licht and Narasimhamurty [8] measured the terminal speed of carbon tetrachloride droplets in water in a vertical column, six inches in diameter. When the equivalent radius of the drop was 0.29 cm the velocity was 19.6 cm/sec. The relevant properties were σ = 41.6 dynes/cm, ρ_d = 1.584 g/ml, $\Delta\rho$ = 0.587 g/ml, ρ_c = 0.997 g/ml, μ_c = 0.894 cP, μ_d = 0.9296 cP.

To apply the theory we first calculate P using eqn. (10)

$$P = \frac{41.6^3 \times 0.997^2}{(0.00894)^4 \times 981 \times 0.587} = 1.95 \times 10^{10}$$

Then r^* is calculated from (8)

$$r^* = 0.29 \left(\frac{0.997 \times 981 \times 0.587}{0.00894^2} \right)^{1/3} = 56$$

Looking at Fig. 10 we see that the point of interest is near the transition between Regions 3 and 4. For Region 3, we have

$$v^* = \sqrt{2}\, r^{*-1/2}\, P^{1/6} = 9.8$$

while for Region 4

$$v^* = \sqrt{2}\, P^{1/12} = 10.2$$

The actual observed value of v^* is derived from the data by using eqn. (7),

$$v^* = 19.6 \left(\frac{0.997^2}{0.00894 \times 981 \times 0.587} \right)^{1/3} = 11.3$$

Thus the measured velocity is about 11% above the predicted value. However, in this transition region we expect that a value of K = 1.56, used in eqn. (23), might give a better estimate. In this case the predicted value of v^* is 11.25, very close to the measured value.

Example 2. Thorsen, Stordalen and Terjesen [21] measured the terminal speed of clean ethylene bromide drops in water at 25°C. A drop with radius 0.064 cm had a speed of 24.65 cm/sec, while one with radius 0.1015 cm traveled at 27.15 cm/sec.

The relevant property values were σ = 31.9 dynes/cm, ρ_c = 0.997 g/cc, $\Delta\rho$ = 1.173 g/cc, μ_c = 0.894 cP.

Proceeding as in Example 1 we find that P = 4.39×10^9 and the experimental values in dimensionless form are:

Point A r^* = 15.55, v^* = 11.3
Point B r^* = 24.66, v^* = 12.46

These points fall in the region between Regions 2 and 3. Since the fluid is said to be "clean" it is appropriate to use eqns. (19) and (22), choosing the lower predicted value in each case.

For point A, using r^* = 15.55, we predict v^* = 12.1 from (19) and v^* = 14.6 from (22). The lower value overestimates the observed result by 7%.

For point B, using r^* = 24.66, we predict v^* = 30.4 from (19) and v^* = 11.6 from (22). The observed value is high by 7%.

Example 3. Haberman and Morton [11] studied air bubbles rising in clean methyl alcohol. Some points from the curve shown in their report are

r (cm)	0.025	0.04	0.068	0.1	0.17	0.3
v (cm/sec)	12	25	25	21	18	20

The property values are μ_c = 0.0052 poise, $\rho_d \simeq 0$, ρ_c = 0.782 g/cc, σ = 21.8 dynes/cm. P is found to be 1.12×10^{10} and the values of the data in dimensionless form are

r^*	7.02	11.23	19.1	28.1	47.8	84.4
v^*	6.34	13.2	13.2	11.1	9.5	10.56

The first two points should fall in Region 2A for which an upper bound is given by (15) with (16) giving a lower estimate. The predictions are

	r^*	7.02	11.23
v^*	(15)	7.6	15.4
v^*	(16)	4.03	7.3

The data fall between the predictions, neither of which is particularly accurate.

The third point falls in Region 3. The predicted value of v^* is 15.3, an overestimate by 16%.

The fourth point lies near the transition between Regions 3 and 4. For Region 3, (22) gives $v^* = 12.6$, while (23) gives $v^* = 9.7$ for $K = \sqrt{2}$ and $v^* = 10.7$ for $K = 1.56$. The observed value of $v^* = 11.1$ is very close to the mean of the three predictions.

The fifth point lies at the minimum velocity point and is very close to the value $v^* = 9.7$ predicted by (23) using $K = \sqrt{2}$.

The final point lies in the transition region between Regions 4 and 5. For Region 4 we predict $v^* = 9.7$ using $K = \sqrt{2}$ and $v^* = 10.7$ using $K = 1.56$. The prediction for Region 5 is $v^* = 9.2$. Again, the best estimate is obtained by using $K = 1.56$ in (23). As a check we calculate the Bond Number and find that $B = (981 \times 0.3^2 \times 0.782)/21.8 \simeq 3.2$, which is consistent with the observation that the prediction using the theory for Region 5 is slightly less than the prediction assuming that Region 4 is appropriate.